Electron Transport in Porous Nanocrystalline TiO 2 Photoelectrochemical Cells

ARTICLE *in* THE JOURNAL OF PHYSICAL CHEMISTRY · OCTOBER 1996

Impact Factor: 2.78 · DOI: 10.1021/jp9616573

4 AUTHORS, INCLUDING:

Peter Searson
Johns Hopkins University
297 PUBLICATIONS **11,813** CITATIONS

SEE PROFILE

Electron Transport in Porous Nanocrystalline TiO_2 Photoelectrochemical Cells

Fei Cao, Gerko Oskam, Gerald J. Meyer,† and Peter C. Searson*

Department of Materials Science and Engineering, The Johns Hopkins University, Baltimore, Maryland 21218

Received: June 5, 1996[⊗]

The photocurrent response of dye-sensitized, porous nanocrystalline TiO_2 cells was studied as a function of light intensity, in both the time domain (photocurrent transient measurements) and the frequency domain (intensity-modulated photocurrent spectroscopy). The photocurrent transients are characterized by a fast and a slow component. The rise time of the transients was in the range of milliseconds to seconds and exhibited a power law dependence on light intensity with an exponent of −0.6 to −0.8. The response to a modulated light intensity is characterized by a depressed semicircle in the complex plane. The time constant obtained from these spectra exhibits the same power law dependence on light intensity. The transient response of these cells is dominated by electron transport in the TiO_2 film, and the results are shown to be consistent with a diffusion model where the diffusion coefficient for electrons in the particle network is a function of the light intensity.

Introduction

Many recent innovations in photoelectrochemical solar energy conversion have been based on the use of porous nanocrystalline films.[1−5] These films are usually comprised of a three-dimensional network of interconnected nanometer-sized particles and exhibit many unique optical and electrical properties in comparison to planar single-crystal or polycrystalline films.

Nanometer-sized particles are generally too small to sustain significant electric fields so that charge separation must be achieved by some other means. In one approach, sub-bandgap illumination may be used to excite dye molecules attached to the surface of the particles. The excited state of the dye molecule injects an electron into the particle, and the dye is regenerated by an electron donor in the solution. Minority carriers are not involved in this process so that electrons may be collected with high efficiency as long as recombination in the form of electron transfer to an electron acceptor in the solution or to the oxidized form of the dye can be minimized. Dye-sensitized, nanoporous TiO_2 photoelectrochemical cells are an example of this approach, and remarkably high-energy conversion efficiencies have been achieved.[1] In another approach, electron−hole pairs generated by direct absorption are separated kinetically. For example, the presence of an efficient hole acceptor in the solution can minimize direct electron−hole recombination in the film.[4] In both cases, only majority carriers are involved in charge transport in the film. Due to the small particle size, electron transport in the network of particles is expected to be dominated by a gradient in the chemical potential of the electrons (diffusion) rather than by an electrical potential gradient (drift). In terms of energetics, transport is dominated by a gradient in the quasi-Fermi level for electrons.

Another unique property of porous nanocrystalline films compared to single-crystal materials is the high surface area. This is an important feature for the dye sensitization approach since high dye coverage is critical to obtaining high absorption coefficients for the films and hence high conversion efficiencies.[1] This feature is also important for the case of direct absorption since the photogenerated holes can be easily removed by hole acceptors in the solution.

Previous studies on dye-sensitized TiO_2 photoelectrochemical cells have shown that the photocurrent transient response is relatively slow with time constants on the order of milliseconds to seconds.[6,7] In contrast, the rate of electron injection into the TiO_2 electrode from the excited state of the dye molecule is a very fast process with time constants on the order of 10^{-9} s or smaller.[8] As a result, the transient response of devices based on porous nanocrystalline films is expected to be dominated by electron transport through the particle network.

Sodergren et al.[9] have proposed a diffusion model for electron transport in these porous films. In this model, the electron diffusion length is assumed to be a constant throughout the film, which is a consequence of the assumptions that the diffusion coefficient and electron lifetime are independent of the electron concentration. The steady-state mass balance equation for electrons in the film was solved, and the calculated photoaction spectra and current−voltage characteristics of the TiO_2 films were shown to be in good agreement with experimental results.

Although many features of photoprocesses can be determined from steady state measurements, a complete analysis of carrier transport can only be obtained from non-steady-state measurements. In this paper, we report on photocurrent transient measurements and intensity-modulated photocurrent spectroscopy (IMPS) of dye-sensitized porous nanocrystalline TiO_2 photoelectrochemical cells. The transient response is dominated by electron transport in the film and can be explained by a diffusion model where the diffusion coefficient for electrons in the particle network is a function of the light intensity.

Experimental Section

The TiO_2 photoelectrodes were prepared in the following way.[10] The TiO_2 powder (Degussa P25) was added to a small amount of water and surfactant (Triton X-100), and the colloidal solution was then applied to a conducting tin oxide glass substrate (8 Ω/□). The film was then sintered for about 30 min at 450 °C after air-drying.

The dye molecule 4,4′-$(dcb)_2Ru(SCN)_2$[5] was attached to the TiO_2 photoelectrodes by immersion in an ethanol solution with a dye concentration of about 0.1 mM for a period of 24 h or more. The polymer gel electrolyte was prepared by refluxing a mixture of 1.4 g of polyacrylonitrile, 10 g of ethylene carbonate, 5 mL of propylene carbonate, 5 mL of acetonitrile,

† Department of Chemistry.

⊗ Abstract published in *Advance ACS Abstracts,* October 1, 1996.

S0022-3654(96)01657-7 CCC: $12.00

1.5 g of NaI, and 0.1 g of I_2. Propylene carbonate and acetonitrile were distilled, and polyacrylonitrile, ethylene carbonate, and NaI were dried in vacuum prior to use. The gel electrolyte was cast onto the dye-coated TiO_2 film and was pressed together with a platinum-coated tin oxide glass counter electrode under N_2 atmosphere in a glovebox. The conductivity of the polymer gel changes as the volatile components in the electrolyte evaporate. The conductivity reached a plateau of about 4×10^{-3} S cm^{-1} after 70 h.[11] The final conductivity of the electrolyte in its gel form was about half of the initial value when the electrolyte was still in its liquid form. In our experiments, the edges of the cells were sealed with epoxy after 3 days of gelation to avoid intrusion of moisture.

The transient measurements were performed using the 514 nm line from a 5 W argon ion laser. The laser beam passed through a beam expander and a beam splitter. A calibrated photodiode was used to monitor the light intensity. The intensity of the light was varied by adjusting the laser output and using a set of neutral density filters. An Isomet Model 120iE acoustooptic modulator driven by a Solartron 1255 HF frequency response analyzer was used as a shutter; the response time was faster than 1 μs. A Newark 846 electromechanical shutter with a rise time of about 4 ms was also used in some slow transient experiments. A PAR 273 potentiostat was used to measure the current, and a digital oscilloscope was used to record the transient signals.

In the IMPS measurement, the acoustooptic modulator driven by the Solartron 1255 frequency response analyzer was used to generate a sinusoidally modulated light intensity. The modulated light intensity and the resulting photocurrent were analyzed by a Solartron 1255 HF frequency response analyzer to obtain the complex quantum efficiencies $\Phi(\omega)$. All photoelectrochemical measurements were performed with the TiO_2 electrodes biased at 0 V, which is in the range of the photocurrent plateau. The cells were illuminated through the conducting glass substrate of the TiO_2 photoelectrodes. No corrections were made for reflection or transmission losses from the cell. The attenuance of the tin oxide conducting glass is about 30% at the experimental wavelength.

Results

Figure 1 shows examples of photocurrent transients under monochromatic ($\lambda = 514$ nm) illumination at 0.05 and 4 mW cm^{-2}. At an illumination intensity of 0.05 mW cm^{-2}, the steady-state photocurrent density was 6 μA cm^{-2} and the rise time was 60 ms. The rise time $t_{1/2}$ is defined by the time at which the current reaches half the steady-state value. At very low light intensity the rise time was longer than 1 s. On increasing the light intensity, the rise time becomes progressively shorter, as can be seen in Figure 1b, which shows a photocurrent transient at 4 mW cm^{-2} where the steady-state photocurrent density is 0.4 mA cm^{-2} and the rise time is 8 ms. At very high light intensities the transient response exhibits a subsequent decay due to diffusion-limited transport of the redox couple in the electrolyte.[6]

Figure 2 shows the steady-state photocurrent and the maximum photocurrent plotted versus the incident light intensity. The maximum photocurrent is linear with the light intensity up to the highest light intensity in our experiments. The current maxima correspond to an incident photon to current conversion efficiency of about 20% through the whole light intensity range. This cell exhibits a threshold light intensity of about 10 mW cm^{-2} below which the photocurrent maximum corresponds to the steady-state value; at higher light intensities the photocurrent rise is followed by a decay process due to limiting transport of the redox couple in the electrolyte. The threshold light intensity is an indicator of the optimum operational limit of the cell. A threshold light intensity of 10−50 mW cm^{-2} was usually observed, which is slightly smaller than the solar intensity at AM1, implying that the operation of these cells would be more efficient under diffuse sunlight.

Figure 3 shows the photocurrent rise at a light intensity of 4 mW cm^{-2} on a semilogarithmic plot. In this plot, a simple exponential rise would yield a straight line from which the time constant of the transient could be determined. The photocurrent

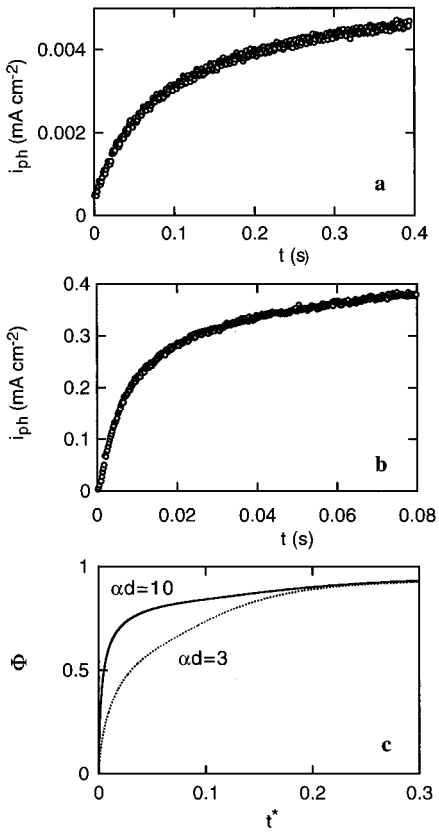

Figure 1. Photocurrent transients recorded under monochromatic (514 nm) illumination at a light intensity of (a) 0.05 and (b) 4 mW cm^{-2}. The TiO_2 electrodes were biased at 0 V. (c) Photocurrent transients calculated according to eq 4 for $\alpha d = 10$ and $\alpha d = 3$. The values for β used in the calculation were 1000 and 300, respectively, and were chosen to correspond to the same light intensity. The abscissa is dimensionless time t^* defined by $t^* = D_0 t/d^2$, and the ordinate is the quantum efficiency Φ. Recombination is neglected in the calculation ($\tau_0 \rightarrow \infty$).

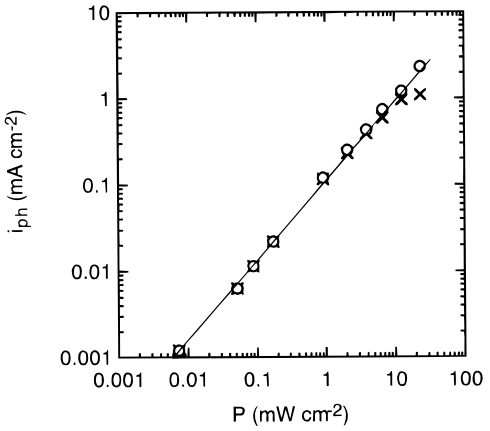

Figure 2. Photocurrent maximum (○) and the steady-state photocurrent (×) plotted versus monochromatic (514 nm) light intensity. The TiO_2 electrodes were biased at 0 V.

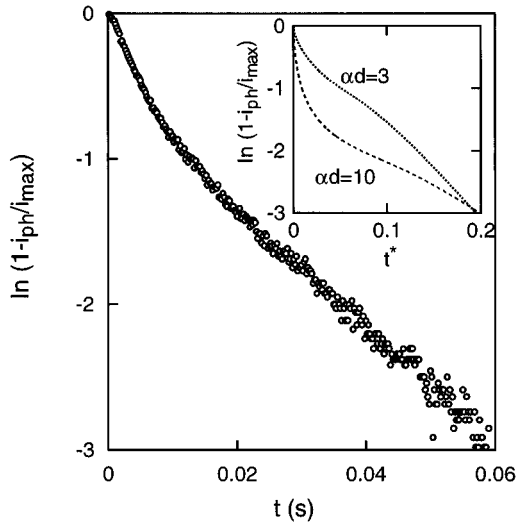

Figure 3. Semilogarithmic plot of a photocurrent transient under monochromatic (514 nm) illumination at 4 mW cm^{-2}. The inset shows a semilogarithmic plot of the calculated photocurrent transients from Figure 1c.

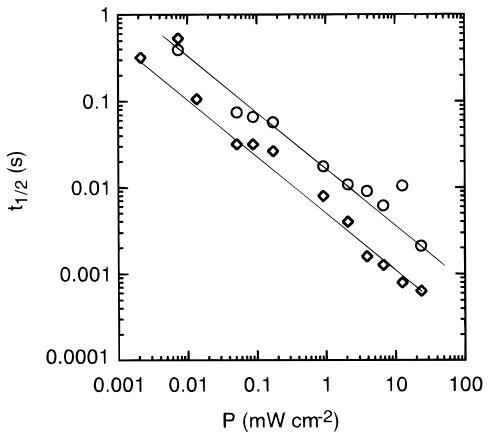

Figure 4. Photocurrent rise time (○) and IMPS time constant (◇) of a TiO_2 cell biased at 0 V versus the monochromatic (514 nm) light intensity.

rise, shown in Figure 3, is characterized by a fast component and a slow component illustrated by the two nearly linear regions in the plot. The linear region of the fast component usually extends over more than one time constant in the semilogarithmic plot, showing that the transient response is dominated by the fast component. The rise time of the fast component was generally found to be from several times to an order of magnitude smaller than that of the slow component. We will show in the next section that the two components are derived from diffusion-controlled electron transport in the film.

Figure 4 shows that the rise times exhibit a power law dependence on light intensity with a slope of −0.7. The rise times ranged from milliseconds to seconds over a light intensity range of almost 3 orders of magnitude. The exponent varied from sample to sample but for all experiments was in the range −0.6 to −0.8. Similar results were obtained for cells with liquid electrolyte.

Figure 5a shows a complex plane plot of the complex quantum efficiency $\Phi(\omega)$ measured at a base light intensity of 4 mW cm^{-2}. At high frequencies $\Phi(\omega)$ is close to zero, indicating that electrons injected into the TiO_2 film cannot reach the back contact, and as a result, a modulated photocurrent is not observed in the external circuit. At very low frequencies $\Phi(\omega)$ is about 17%, which is close to the steady-state quantum

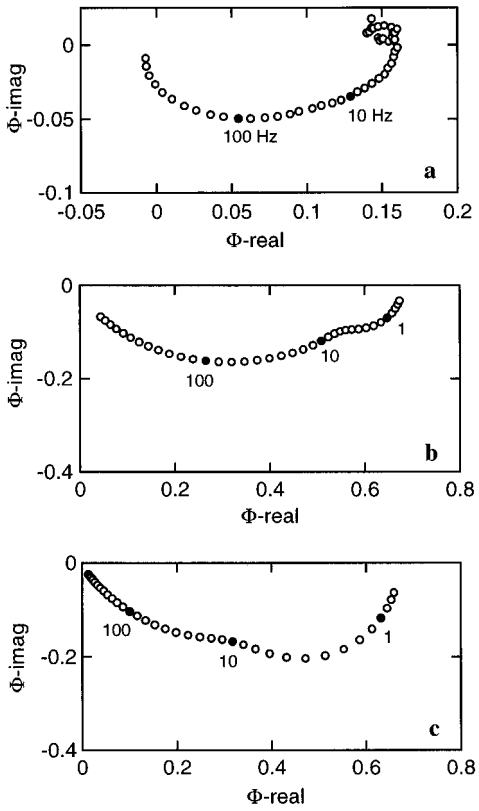

Figure 5. (a) Complex plane plot of the IMPS response of a TiO_2 cell at a base light intensity of 4 mW cm^{-2}. Complex plane IMPS response calculated according to eq 4 (see Appendix C) for (b) $\alpha d = 10$ and $\beta = 1000$ and (c) $\alpha d = 3$ and $\beta = 300$. In (b) and (c) the frequencies are in dimensionless units.

efficiency. At intermediate frequencies a depressed and distorted semicircle is observed.

In general, at light intensities below the characteristic threshold intensity, the high-frequency value for $\Phi(\omega)$ was close to zero and the low-frequency value was equal to the steady-state efficiency. At higher light intensities, a small depressed semicircle was observed in the first quadrant corresponding to the decay process seen in the transients. In this case, the intercept with the real axis at the low-frequency limit corresponded to the steady-state quantum efficiency.

In IMPS measurements, a single time constant process would result in a semicircle in a complex plane plot of the quantum efficiency where the frequency at the apex of the semicircle can be related to the time constant of the process.[12,13] The observed depressed semicircle indicates a nonexponential or multi-time constant process consistent with the transient measurements. The time constant $\tau = (2\pi f_{max})^{-1}$ determined from the frequency at the imaginary maximum at a base light intensity of 4 mW cm^{-2} was 1.5 ms. The IMPS time constants follow a similar power law relationship with light intensity as the rise times of the transients, as shown in Figure 4. From this figure it can also be seen that the time constants obtained from the IMPS measurements were generally smaller than the time constants obtained from photocurrent transients at the same light intensity.

Discussion

A characteristic feature of the porous nanocrystalline TiO_2 photoelectrochemical cells is the slow photocurrent transients with rise times on the order of milliseconds to seconds depending on light intensity. Several considerations lead to the conclusion that the transient response is dominated by electron

transport in the TiO_2 film. First, the rise time associated with the photocurrent transient is more than 6 orders of magnitude slower than the rate of electron injection from the excited dye molecule to the TiO_2 particles. Second, transport of the redox couple in the electrolyte only contributes to the transient response at high light intensity where an additional decay is observed.

Carrier transport in the semiconductor film can be described by the continuity equation[14]

$$\frac{\partial n}{\partial t} = \frac{1}{e}\frac{\partial J}{\partial x} + G - R \quad (1)$$

where n is the electron density under illumination, J is current density in the film, and G and R are the carrier generation rate and recombination rate, respectively. In the dye-sensitized porous TiO_2 film, the generation rate can be written as $G = \Gamma\alpha \exp(-\alpha x)$, where Γ is the photon flux and α is the wavelength-dependent absorption coefficient of the dye-sensitized film. This implies that the dye concentration is uniform throughout the film. Recombination is assumed to be proportional to the electron concentration and can be written as $R = (n - n_0)/\tau_0$, where n_0 is the electron density in the dark and τ_0 is the position-independent electron lifetime. Both electron drift and diffusion can contribute to the current density:

$$J = en\mu_n \frac{\partial \phi}{\partial x} + eD\frac{\partial n}{\partial x} \quad (2)$$

where μ_n is the electron mobility, ϕ is the electrical potential in the film, and D is the diffusion coefficient of electron. Since the TiO_2 particles are too small to sustain significant band bending, the current density is expected to be dominated by the diffusion term. The reconfiguration of electrons in the TiO_2 film will lead to an electrical field that is not related to the band bending in the individual particles. At relatively low light intensities where the electron density is not too high, the electrical field in the TiO_2 film can be neglected. The time-dependent transport equation for electrons is obtained by substituting eq 2 into eq 1. In the absence of electron migration, the continuity equation becomes

$$D\frac{\partial^2 n(x,t)}{\partial x^2} - \frac{\partial n(x,t)}{\partial t} - \frac{n(x,t) - n_0}{\tau_0} + \Gamma\alpha \exp(-\alpha x) = 0 \quad (3)$$

The first two terms represent the electron flux and the change in electron concentration with time, respectively. The third term represents the recombination rate and is characterized by the time constant τ_0. The fourth term is the rate of electron injection from the photoexcitation process. Equation 3 can be solved analytically by separation of variables and Fourier transformation. The solution is shown in Appendix A.

The solution to eq 3 predicts that the steady-state photocurrent is proportional to the light intensity in agreement with the model of Sodergren et al.[9] and is consistent with the experimental observations shown in Figure 2. It can be seen from eqs A2−A4 that the solution gives a nonexponential rise and that the characteristic rise time is independent of light intensity as indicated by the absence of the photon flux Γ in the exponential terms. The recombination term only modifies the rise time of the transients; it does not change the essential features of the solution. These results, however, contradict the experimental observation, shown in Figure 4, that the rise time becomes progressively shorter with increasing light intensity. Consequently, eq 3 does not adequately describe the transient behavior of the TiO_2 films.

The diffusion coefficient D of electrons in the film does not correspond to the transport of free electrons in the conduction band of single-crystal TiO_2. Based on an electron mobility of about 1 $cm^2\ V^{-1}\ s^{-1}$,[15] the diffusion coefficient for free electrons determined from the Einstein equation is on the order of 10^{-2} $cm^2\ s^{-1}$ at room temperature, much larger than the values suggested from the slow transients reported here. This result implies that the diffusion coefficient represents the thermally activated transport of electrons through the particle network. Two examples of related processes are outlined below.

In amorphous and disordered semiconductors, it is well-known that charge trapping can give rise to very slow phototransient processes.[16,17] These materials are characterized by a high density of trap sites, and consequently, charge transport is often dominated by the properties of the traps. In many cases the traps are distributed over a broad energy range so that the electron mobility is dependent on trap occupancy (Fermi level) and hence on the electron density. Another example involves polycrystalline CdS and CdSe films fabricated from sintered powders. These films are characterized by high-conductivity particles separated by photosensitive, low-conductivity contact regions.[18] On illumination, the resistance of the contact regions may be reduced resulting in an increase in the electron mobility and hence the current density.

Taking these considerations into account, the diffusion coefficient D for electrons in the film is assumed to be proportional the the electron concentration. Neglecting recombination losses, the transport equation for electrons becomes

$$\frac{\partial\left(D_0 \dfrac{n(x,t)}{n_0}\dfrac{\partial(n(x,t))}{\partial x}\right)}{\partial x} - \frac{\partial n(x,t)}{\partial t} + \Gamma\alpha \exp(-\alpha x) = 0 \quad (4)$$

where D_0 is the diffusion coefficient in the dark, and $n(x,t)$, n_0, Γ, and α have the same meaning as before.

A numerical solution for eq 4 was obtained using a forward time central space (FTCS) algorithm. The solution, summarized in Appendix B, is described in terms of two dimensionless parameters γ and β. The parameter γ describes the absorbance of the film and is given by $\gamma = \alpha d$, where d is the film thickness. The term $\beta = \Gamma\alpha d^2/n_0 D_0$ and is proportional to the light intensity. Figure 1c shows calculated transients for $\alpha d = 10$ and $\alpha d = 3$.[19] The β values of 1000 and 300, respectively, were chosen to give the same photon flux. The inset in Figure 3 shows these transients on a semilogarithmic plot. For the case where $\alpha d = 10$, corresponding to strong absorption, the photocurrent rise is characterized by two components with the initial fast component extending over more than one time constant in the semilogarithmic plot. These features are consistent with the experimental observations. For the case where $\alpha d = 3$, corresponding to a relatively weak absorption, the transition between the two processes is not as distinct. This is due to the fact that fewer electrons are injected in the vicinity of the back contact, thus slowing down the fast component of the photocurrent rise, while more electrons are injected in the outer portion of the film, thus speeding up the slow component.

Figure 6 shows the evolution of the electron concentration profiles, calculated from eq 4, for the transients shown in Figure 1c. The concentration profile during the fast part of the transient is characterized by a steady buildup of a concentration peak within a short distance of the back contact. In the slow process, the electron concentration in the outer portion of the film builds up to the steady-state concentration profile. In the absence of recombination of electrons with acceptors in the electrolyte the concentration peak moves to the outer part of the film, resulting

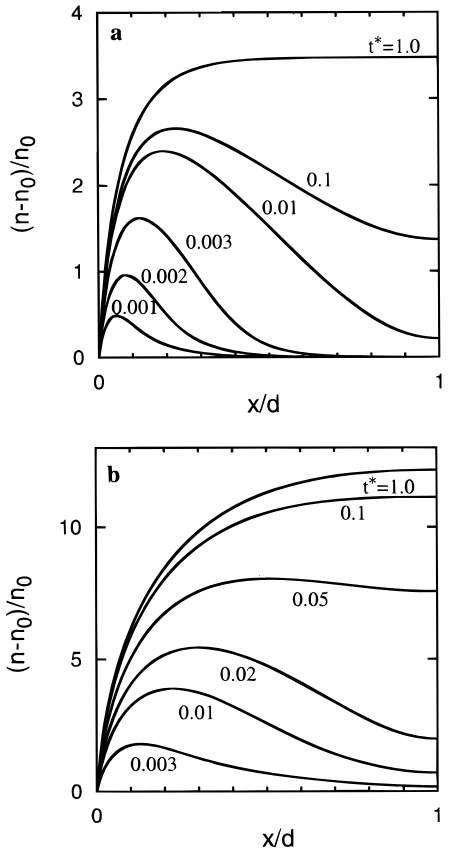

Figure 6. Calculated spatial distribution of the electron concentration in the film obtained from eq 4 as a function of dimensionless time t^* for (a) $\alpha d = 10$, $\beta = 1000$ and (b) $\alpha d = 3$, $\beta = 300$.

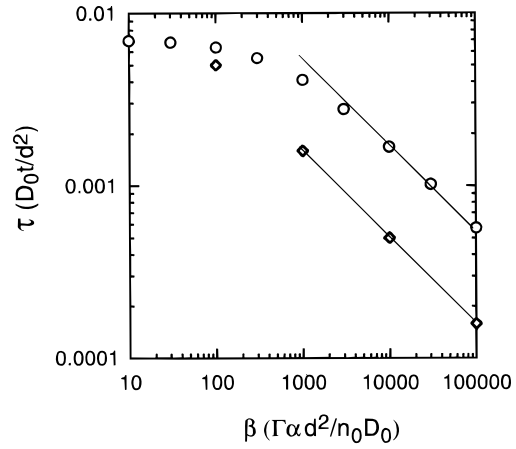

Figure 7. Dimensionless photocurrent rise times (○) and IMPS time constants (◇) calculated from eq 4 plotted versus β. For all calculations $\alpha d = 10$.

in a monotonic distribution of electron density in the electrode with the outer part of the film having the highest electron concentration. For the case of relatively weak absorption in the film ($\alpha d = 3$), the concentration peak is far away from the back contact, and the initial increase of the peak is much less pronounced. These results show that the fast and slow components of the transients reflect the variation of absorption efficiencies of different dye-sensitized TiO_2 films.

Figure 7 shows a logarithmic plot of the rise time, $t_{1/2}$, of the calculated transients as a function of the incident light intensity in terms of the dimensionless absorption coefficient γ and the dimensionless light intensity β. The rise times of the calculated transients exhibit a power law dependence on light intensity with a slope of -0.5, similar to the experimental results shown in Figure 4. At the low light intensity limit, the time constant reaches a plateau corresponding to the condition where $n \rightarrow n_0$ and $D \rightarrow D_0$. A low light intensity for the onset of the rise time plateau is an indicator of low dopant density in the film. Experimentally, this plateau was not observed, and time constants longer than 1 s were seen at very low light intensities. These observations give an upper limit for the dark diffusion coefficient D_0 of 10^{-7} cm^2 s^{-1}, much smaller than the value for transport of free electrons in single-crystal TiO_2. In addition, we obtain an upper limit for the product n_0D_0 on the order of 10^9 cm^{-1} s^{-1}.

The features of the simulation can be changed by further modifying the diffusion equation. The slope in Figure 7 is related to the concentration dependence of the diffusion coefficient, and it can be shown that if $D \propto n^{\eta}$, then the slope is given by $-\eta/(1 + \eta)$. A stronger concentration dependence of the diffusion coefficient will increase this slope corresponding to a stronger dependence of the photocurrent rise time on the light intensity.

Introducing a recombination term into eq 4 has little effect on the fast component of the transient but suppresses the slow part since electrons in the outer part of the film will recombine before reaching the back contact and contributing to the current. In this case the slow process is removed from the transient behavior, resulting in an overall faster transient response and lower steady-state current. The inclusion of the recombination term also leads to a peak in the steady-state electron concentration profile in the film. The appearance of the slow part of the transient is itself indicative of a relatively long lifetime for electrons in these films.

The IMPS response can be also calculated for the diffusion-controlled transport model with $D \propto n(\eta{=}1)$. The calculation is summarized in Appendix C. Figure 5b shows a complex plane plot of the IMPS spectrum calculated for $\alpha d = 10$, revealing two relaxation processes corresponding to the fast and slow components seen in the both experimental and calculated photocurrent transients. The time constant associated with the imaginary maximum corresponds to the fast component while the time constant associated with the lower frequency semicircle is associated with the slower component. For the case of strong absorption ($\alpha d = 10$) the two processes are clearly seen in the complex plane plot. The complex plane IMPS spectrum obtained for $\alpha d = 3$ at the same light intensity (Figure 5c) shows that the difference between the time constants of the two components becomes smaller when the absorption depth becomes sufficiently large. Experimentally, the separation between the two processes is not clearly distinguishable as seen in Figure 5a. The calculations presented here show two limiting cases and are not intended to give the best fit of the experimental data.

The time constant obtained from the frequency at the imaginary maximum for $\alpha d = 10$ decreases as the light intensity increases, as shown in Figure 7. The time constant from the calculated IMPS response is shorter than the calculated transient rise time consistent with the experimental observation shown in Figure 3. In the transient measurements, an electron concentration gradient has to be built up from the dark electron density in the film, which makes the photocurrent rise a rather slow process. In the IMPS measurement, the existing steady-state electron concentration increases the diffusion coefficient, leading to a smaller time constant in the IMPS measurement.

Conclusions

The photocurrent transients observed for dye-sensitized nanoporous TiO_2 films are relatively slow. Under backside

illumination, the photocurrent rise is characterized by a fast component due to injection of carriers close to the contact and a slow component related to the buildup of the electron concentration gradient in the film to a steady-state value. The fast component dominates the transient response and extends over more than one time constant on a semilogarithmic plot. The rise time of the photocurrent transient exhibits a power law dependence on light intensity with an exponent of −0.6 to −0.8. The time constants obtained from IMPS measurements exhibit the same dependence, although the values were smaller than those obtained from transient measurements at the same light intensity.

The essential features of the non-steady-state response can be described by a diffusion model where the electron diffusion coefficient is dependent on light intensity. Physically, this model is consistent with an electron transport process controlled by thermal excitation from trap states in the particles. We emphasize that the diffusion coefficient D is expected to be a function of the sample morphology and preparation methods. Finally, we note that this model can also be applied to porous nanocrystalline electrodes without dye sensitization, provided that the photogenerated holes are removed rapidly.

Acknowledgment. The authors thank Dr. Gang Bao for guidance in obtaining the analytical solution to the transport equation given in Appendix A. The authors also thank Jeremy Stipkala and Todd Heimer for providing the dye molecules. This work was supported by the National Renewable Energy Laboratory under Subcontract XAD-3-12114-04.

Appendix A

The transport equation for electrons in the TiO_2 film in the absence of an electric field can be written as

$$D\frac{\partial^2 n(x,t)}{\partial x^2} - \frac{\partial n(x,t)}{\partial t} - \frac{n(x,t) - n_0}{\tau_0} + \Gamma\alpha \exp(-\alpha x) = 0 \quad \text{(A1)}$$

where n is the electron density under illumination, n_0 is the electron density in the dark, Γ is the photon flux, τ_0 is the mean electron lifetime, and α is the absorption coefficient of the film at the experimental wavelength. The boundary conditions are

$$n(x{=}0,t) = n_0, \quad n(x,t{=}0) = n_0, \quad \left(\frac{\partial n(x,t)}{\partial x}\right)_{x=d} = 0$$

where d is the film thickness.

Equation A1 can be solved by separation of variables and Fourier transformation. The time-dependent photocurrent $J(t)$ can be written as

$$J(t) = eD\left(\frac{\partial n(x,t)}{\partial x}\right)_{x=0} =$$

$$J_{SS} - \sum_{k=0}^{\infty} C_k \frac{\pi}{2d}(2k+1)\exp\left(-\left(\frac{1}{\tau_0} + \frac{D\pi^2(2k+1)^2}{4d^2}\right)t\right) \quad \text{(A2)}$$

where J_{SS} is the steady-state photocurrent and is given by

$$J_{SS} = \frac{e\Gamma\alpha L\left(-\sinh\left(\frac{d}{L}\right) - \alpha L \exp(-\alpha d) + \alpha L \cosh\left(\frac{d}{L}\right)\right)}{(L^2\alpha^2 - 1)\cosh\left(\frac{d}{L}\right)} \quad \text{(A3)}$$

where $L = \sqrt{D\tau_0}$ and C_k is given by

$$C_k = \frac{2e\Gamma\alpha L^2}{d(1 - L^2\alpha^2)}\left(\frac{(-1)^{k+1}\alpha \exp(-\alpha d) + \frac{\pi}{2d}(2k+1)}{\frac{1}{L^2} + \frac{\pi^2(2k+1)^2}{4d^2}} + \frac{(-1)^k\alpha \exp(-\alpha d) - \frac{\pi(2k+1)}{2d}}{\alpha^2 + \frac{\pi^2(2k+1)^2}{4d^2}}\right) \quad \text{(A4)}$$

From consideration of eqs A2−A4 it can be seen that the normalized photocurrent transient, $J(t)/J_{SS}$, is not a function of the photon flux Γ. The transient time constant is, therefore, independent of light intensity.

Appendix B

Taking the diffusion coefficient D to be proportional to the electron concentration and neglecting recombination with acceptors in the electrolyte, the electron transport equation is given by

$$\frac{\partial\left(D_0\frac{n(x,t)}{n_0}\frac{\partial(n(x,t))}{\partial x}\right)}{\partial x} - \frac{\partial n(x,t)}{\partial t} + \Gamma\alpha \exp(-\alpha x) = 0 \quad \text{(B1)}$$

where D_0 is the electron diffusivity in the dark. All other parameters have the same meaning as before.

We define the dimensionless electron concentration, n^*, dimensionless distance, x^*, and dimensionless time, t^*, as

$$n^* = \frac{n}{n_0}, \quad x^* = \frac{x}{d}, \quad t^* = \frac{D_0 t}{d^2}$$

Substituting these parameters into eq B1, we obtain

$$n^*\left(\frac{\partial^2 n^*}{\partial x^{*2}}\right) + \left(\frac{\partial n^*}{\partial x^*}\right)^2 - \frac{\partial n^*}{\partial t^*} + \beta \exp(-\gamma x^*) = 0 \quad \text{(B2)}$$

where $\beta = \Gamma\alpha d^2/n_0 D_0$ and $\gamma = \alpha d$.

A numerical solution for eq B2 can be obtained by the forward time central space (FTCS) method, which transforms the differential equation into a recursive relationship by digitizing the time and space variables. Defining $x^* = i\Delta x$ and $t^* = m\Delta t$ where i and m are integers, we then have

$$\left(\frac{\partial^2 n^*}{\partial x^{*2}}\right)_{t^*=m\Delta t,\, x^*=i\Delta x} = \frac{n^*(i+1, m) + n^*(i-1, m) - 2n^*(i, m)}{\Delta x^2} \quad \text{(B3)}$$

$$\left(\frac{\partial n^*}{\partial x^*}\right)_{t^*=m\Delta t,\, x^*=i\Delta x} = \frac{n^*(i+1, m) - n^*(i, m)}{\Delta x} \quad \text{(B4)}$$

$$\left(\frac{\partial n^*}{\partial t^*}\right)_{t^*=m\Delta t,\, x^*=i\Delta x} = \frac{n^*(i, m+1) - n^*(i, m)}{\Delta t} \quad \text{(B5)}$$

Substituting eqs B3−B5 into eq B2, the electron concentration can be solved as a function of time. The normalized current J^* at time $t^* = m\Delta t$ is obtained from

$$J^*(t^*{=}m\Delta t) = n^*\,[n^*(1, m) - 1]/\Delta x \quad \text{(B6)}$$

Appendix C

For the IMPS calculation, a modulated light intensity, $\tilde{\beta}$, is superimposed on a base light intensity β_0. The electron

concentration $n^*(x,t)$ consists of a steady-state term n^*_{SS} and an modulated term $\tilde{n}^*$. The transport equation (B1) under these conditions becomes

$$n^*\left(\frac{\partial^2 n^*}{\partial x^{*2}}\right) + \left(\frac{\partial n^*}{\partial x^*}\right)^2 - \frac{\partial n^*}{\partial t^*} + \beta \exp(-\gamma x^*) = 0 \quad \text{(C1)}$$

where $\beta = \beta_0 + \tilde{\beta}\cos(-\omega t)$ and $n^* = n^*_{SS} + \tilde{n}^*$.

Equation C1 can be separated into a dc component due to the base light intensity

$$n^*_{SS}\frac{\partial^2 n^*_{SS}}{\partial x^{*2}} + \left(\frac{\partial n^*_{SS}}{\partial x^*}\right)^2 + \beta_0 \exp(-\gamma x) = 0 \quad \text{(C2)}$$

and an ac component due to the modulation:

$$(n^*_{SS} + \tilde{n}^*)\left(\frac{\partial^2 n^*_{SS}}{\partial x^{*2}} + \frac{\partial^2 \tilde{n}^*}{\partial x^{*2}}\right) + \left(\frac{\partial n^*_{SS}}{\partial x^*}\right)^2 + 2\left(\frac{\partial n^*_{SS}}{\partial x^*}\right)\left(\frac{\partial \tilde{n}^*}{\partial x^*}\right) + \left(\frac{\partial \tilde{n}^*}{\partial x^*}\right)^2 - \frac{\partial \tilde{n}^*}{\partial t^*} + (\beta_0 + \tilde{\beta}\cos(\omega t))\exp(-\gamma x) = 0 \quad \text{(C3)}$$

A solution for $\tilde{n}^*$ can be obtained using the FTCS method described above. The corresponding modulated photocurrent can be obtained in a similar way. The frequency dependent quantum efficiency is obtained from

$$\Phi(\omega) = \tilde{n}^*/\tilde{\beta} \quad \text{(C4)}$$

References and Notes

(1) O'Regan, B.; Grätzel, M. *Nature* **1991**, *353*, 737.

(2) Meyer, G. J.; Searson, P. C. *Interface* **1993**, *2*, 23.

(3) Cao, F.; Oskam, G.; Searson, P. C.; Stipkala, J. M.; Heimer, T. A.; Farzad, F.; Meyer, G. J. *J. Phys. Chem.* **1995**, *99*, 11976.

(4) Hodes, G.; Howell, I. D. J.; Peter, L. M. *J. Electrochem. Soc.* **1992**, *139*, 3136.

(5) Heimer, T. A.; Bignozzi, C. A.; Meyer, G. J. *J. Phys. Chem.* **1993**, *97*, 11987.

(6) Cao, F.; Oskam, G.; Searson, P. C. In *Nanostructured Materials in Electrochemistry*; Searson, P. C., Meyer, G. J., Eds.; Electrochemical Society: Pennington, NJ; Proc. Vol. 95−8.

(7) Oskam, G.; Cao, F.; Searson, P. C. In *Nanostructured Materials in Electrochemistry*; Searson, P. C., Meyer, G. J., Eds.; Electrochemical Society: Pennington, NJ; Proc. Vol. 95−8.

(8) Eichberg, R.; Willig, F. *Chem. Phys.* **1990**, *141*, 159.

(9) Sodergren, S.; Hagfeldt, A.; Olsson, J.; Lindquist, S. E. *J. Phys. Chem.* **1994**, *98*, 5552.

(10) Nazeeruddin, M. K.; Kay, A.; Rodicio, I.; Humphry-Baker, R.; Muller, E.; Liska, P.; Vlachopoulos, N.; Grätzel, M. *J. Am. Chem. Soc.* **1993**, *115*, 6382.

(11) Cao, F.; Oskam, G.; Searson, P. C. *J. Phys. Chem.* **1995**, *99*, 17073.

(12) Searson, P. C.; Macdonald, D. D.; Peter, L. M. *J. Electrochem. Soc.* **1992**, *139*, 2538.

(13) Li, J.; Peter, L. M. *J. Electroanal. Chem.* **1985**, *193*, 27.

(14) Ryvkin, S. M. *Photoelectric Effects in Semiconductors*; Consultants Bureau: New York, 1994.

(15) Finklea, H. O., Ed. *Semiconductor Electrodes*; Elsevier Science Publishers B. V.: Amsterdam, 1988.

(16) Schwarzburg, K.; Willig, F. *Appl. Phys. Lett.* **1991**, *58*, 2520.

(17) Schmidlin, F. W. *Phys. Rev.* **1977**, *16*, 2362.

(18) Bube, R. H. *Photoconductivity of Solids*; Robert E. Krieger: New York, 1978.

(19) Note that $\alpha d = 10$ would be obtained for a 10 μm thick film with an absorption coefficient of 10^4 cm^{-1}.

JP9616573